

GeoVLMATH: Enhancing Geometry Reasoning in Vision-Language Models via Cross-Modal Reward for Auxiliary Line Creation

Shasha Guo¹, Liang Pang¹, Xi Wang², Yanling Wang³, Huawei Shen¹, Jing Zhang^{2*}

¹Institute of Computing Technology, Chinese Academy of Sciences, China

²Renmin University of China, China ³Zhipu AI, China

{guoshasha, pangliang, shenhuawei}@ict.ac.cn

{wangxi2022, zhang-jing}@ruc.edu.cn, yanlingwang777@gmail.com

Abstract

Auxiliary lines are essential for solving complex geometric problems but remain challenging for large vision-language models (LVLMs). Recent attempts construct auxiliary lines via code-driven rendering, a strategy that relies on accurate and executable code generation to produce visual renderings of the auxiliary lines for subsequent reasoning. However, in complex solid geometry settings, such a strong dependence on precise specifications substantially restricts the robustness of this strategy. Alternatively, we turn to a simpler and more stable solution, representing auxiliary-line constructions as structured textual descriptions. To bridge the gap between textual descriptions and spatial structure, we propose a reinforcement learning framework that enhances diagram-text alignment. The core is a cross-modal reward model that evaluates how well the generated auxiliary-line description matches the ground-truth auxiliary-line diagram. The reward signal drives a GRPO-based RL stage to yield informative auxiliary-line descriptions for the reasoning. To support the training and evaluation, we develop a scalable data pipeline and construct AuxSolidMath¹, a dataset of 3,018 real-exam geometry problems with paired diagrams and aligned textual fields. Based on this framework, we derive GeoVLMATH, an LVLM for solving complex solid geometry.

1 Introduction

Geometric problems constitute an important category of mathematical tasks, characterized by intricate spatial structures and multi-step reasoning processes (Ma et al., 2024). They are commonly divided into plane geometry and solid geometry. This study focuses on solid geometry, where reasoning over three-dimensional spatial relations is

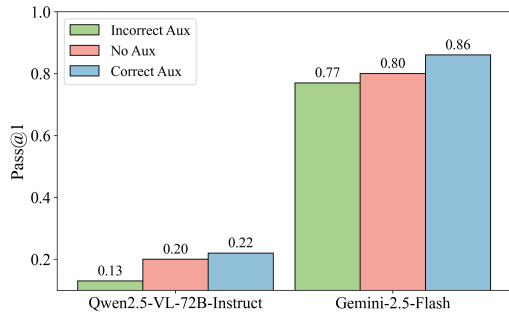


Figure 1: Pass@1 results for Qwen2.5-VL-72B-Instruct and Gemini-2.5-Flash. “Aux” indicates the use of auxiliary-line descriptions.

substantially more complex. Such problems rarely yield to direct application of standard theorems; instead, they often require the deliberate introduction of auxiliary lines² to reveal hidden geometric structure and enable further analysis. These auxiliary lines are essential for anchoring visual diagrams to formal symbolic reasoning and for providing the intermediate steps for rigorous problem-solving.

To validate the above idea, we conduct a pilot study comprising three experimental settings: Incorrect Aux (with incorrect auxiliary lines), No Aux (without auxiliary lines), and Correct Aux (with correct auxiliary lines). As shown in Figure 1, **the use of correct auxiliary lines achieves the highest accuracy, whereas incorrect auxiliary lines lead to the poorest performance**. One possible explanation is that inaccurate auxiliary lines tend to misdirect reasoning and produce errors, while precise auxiliary lines uncover key spatial relationships, thereby enhancing solution accuracy.

Given that accurate auxiliary lines are crucial for the correctness of the solution, the key question is how to obtain them reliably. A seemingly straightforward solution is to explicitly construct them on the diagram. Indeed, several representative methods, such as Visual Sketchpad (Hu et al.,

* Corresponding Author

¹The dataset is now publicly available at <https://huggingface.co/datasets/shasha/AuxSolidMath>

²In this paper, we use *auxiliary lines* broadly to include both additional lines and coordinate systems.

2024), V-Thinker (Qiao et al., 2025), and CodePlot-CoT (Duan et al., 2025), follow a unified paradigm in which the model generates Python-based drawing code to render intermediate diagrams that are then fed back into the reasoning process. Despite its conceptual simplicity, this code-driven visual construction paradigm exhibits inherent limitations in solid geometry. It critically relies on precise coordinate information and highly accurate code generation, and becomes particularly fragile when auxiliary lines involve cross-plane relations or skew structures, where minor rendering inaccuracies can distort spatial constraints and mislead reasoning. Our empirical results corroborate this limitation, **showing that explicitly rendered auxiliary-line diagrams underperform text-based auxiliary-line formulations** (See Table 2).

In light of these observations, we adopt a simpler and more stable formulation by representing auxiliary-line constructions as structured textual descriptions. Our main idea is to design a **cross-modal reward model** that measures the consistency between a generated textual auxiliary-line description for the original diagram and a ground-truth auxiliary-line diagram. The reward is computed by jointly encoding the original diagram and the generated auxiliary-line description, and then comparing this pair with the ground-truth auxiliary-line diagram, providing geometry-aware supervision without requiring coordinate assumptions or image manipulation. Building on this reward signal, we train a policy model using Group Relative Policy Optimization (GRPO) to obtain geometry-consistent, generalizable constructions. Training follows a two-stage paradigm inspired by recent progress in reinforcement learning (RL) for reasoning (e.g., DeepSeek-R1 (Guo et al., 2025)): supervised fine-tuning (SFT) for cold start, followed by GRPO-based RL to further elicit structured reasoning and strengthen diagram-text alignment. We instantiate the framework as GeoVLM, a vision-language model tailored to auxiliary-line-based geometric reasoning. Through the cross-modal supervision, GeoVLM achieves strong alignment between text and geometric structure, enabling faithful reasoning on complex diagrams.

To effectively train the above model, we require a high-quality dataset that captures both visual and symbolic aspects of real-world geometry problems. However, creating such a dataset is inherently challenging due to the need for automation, scalability, and semantic precision across diverse and noisy

educational materials. In response to these challenges, we develop a **robust and scalable data construction pipeline** that transforms raw high school exam papers into structured multimodal instances suitable for training LVLMs, comprising automated problem identification, automated deduplication and diagram extraction, structured data extraction, and manual verification. While the pipeline is largely automated, this lightweight manual verification step is essential for maintaining data quality, particularly when handling complex symbolic expressions and diagrammatic content in real-world settings. Based on this pipeline, we construct **AuxSolidMath**, a curated dataset of 3,018 solid geometry problems in a rich multimodal format, comprising the problem description, the final answer, the auxiliary-line description, the original diagram, and the auxiliary-line diagram. To our knowledge, AuxSolidMath is the first systematically constructed dataset explicitly tailored to auxiliary-line-based solid geometry reasoning.

We empirically evaluate GeoVLM against a broad range of LVLMs, including representative approaches that construct auxiliary lines via code-driven rendering. Despite its relatively modest parameter scale, GeoVLM achieves highly competitive performance, consistently outperforming code-driven rendering methods and surpassing larger models such as Qwen2.5-VL-32B-Instruct (Bai et al., 2025) and GPT-4o (Hurst et al., 2024). These results indicate that supervision grounded in auxiliary-line constructions is more effective for improving geometric reasoning than explicit code-driven diagram rendering or simply scaling model size. Furthermore, our evaluation protocol highlights the value of auxiliary-line-augmented datasets for revealing the limitations of LVLMs in visual reasoning.

Contributions. (1) **Cross-modal reward.** We introduce a geometry-aware scalar reward that directly evaluates diagram-text alignment, providing reliable and fine-grained supervision for reinforcement learning in auxiliary-line construction. (2) **AuxSolidMath.** We introduce AuxSolidMath, a curated dataset of 3,018 solid geometry problems from real high-school exams, with aligned diagrams, auxiliary-line annotations, and answers, designed to support training and evaluation of auxiliary-line reasoning. (3) **GeoVLM.** We introduce GeoVLM, demonstrating that RL with vision-based rewards effectively optimizes

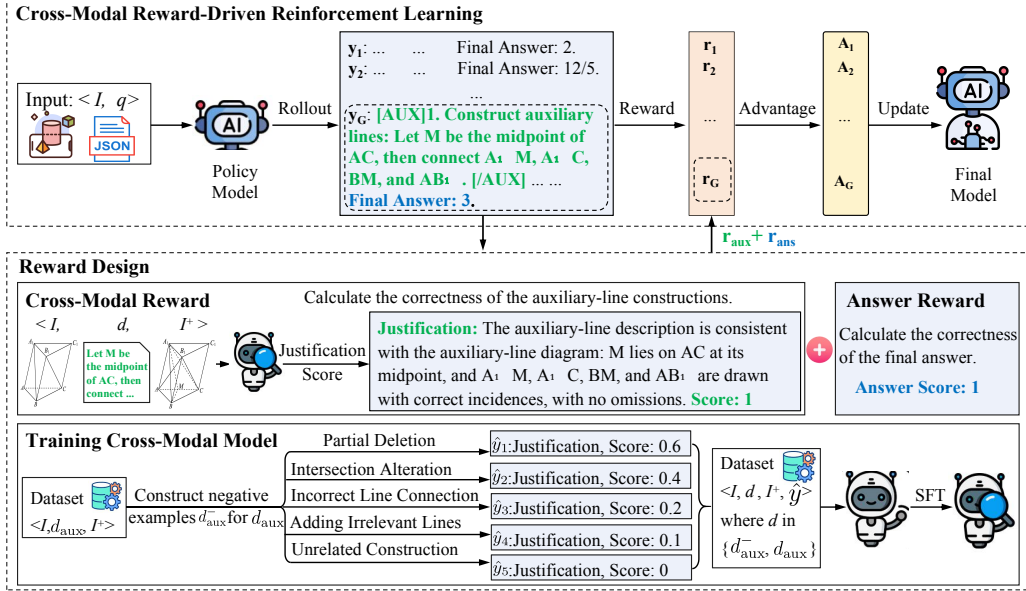


Figure 2: Overview of the cross-modal reward-driven RL. We first fine-tune a cross-modal reward model to evaluate the correctness of auxiliary-line constructions. During the RL phase, the reward model’s consistency score is combined with the answer accuracy reward to produce a composite signal that updates the policy via GRPO.

auxiliary-line construction, achieving superior performance to code-driven rendering approaches and competitive results against larger LVLMs.

2 Methodology

2.1 Problem Definition

We study solid geometry problems whose solutions require the *active construction of auxiliary lines*. Each instance is defined by a pair $\langle I, q \rangle$, where I denotes the original diagram and q is a question grounded in I . The goal is to generate a solution y that includes the auxiliary lines aux , a sequence of reasoning steps, and the final answer ans . The aux is not present in I and must be introduced during reasoning to expose implicit spatial relations and convert them into explicit geometric constraints.

2.2 Framework Overview

We introduce a two-stage training framework for LVLMs that integrates the auxiliary-line construction into the reasoning process. In the first stage, we apply SFT on automatically synthesized chain-of-thought (CoT) data with explicit auxiliary-line steps, enabling the model to actively construct auxiliary lines, thereby establishing a good initialization. In the second stage, we further use RL to encourage the model to construct auxiliary lines that faithfully reflect the geometry of the diagram, boosting the precision of the solution. At the core is a **cross-modal reward model** that provides fine-grained feedback by scoring the agreement

between the original diagram plus the generated auxiliary-line description and a reference diagram annotated with the correct auxiliary line. In summary, our framework combines direct supervision with structured visual feedback, thereby enhancing the reliability of auxiliary-line constructions and overall geometric problem-solving performance.

2.3 Supervised Fine-Tuning

We apply SFT on CoT exemplars to initialize the model for RL. Auxiliary-line construction steps are explicitly marked with **[AUX]** and **[/AUX]** to provide structured supervision and support later reward modeling, and the model is trained using a standard next-token prediction objective.

2.4 Cross-Modal Reward-Driven RL

As shown in Figure 1, accurate auxiliary-line constructions improve reasoning success. The key challenge is how to integrate such constructions into the reasoning process. Recent methods adopt Python-based drawing code to render auxiliary lines for intermediate reasoning, yet their reliance on precise and executable specifications limits robustness in complex solid geometry. Motivated by this limitation, and inspired by recent advances in textual CoT supervision (Xu et al., 2024; Zhang et al., 2025), we represent auxiliary-line constructions as structured natural language descriptions. To bridge the gap between textual descriptions and spatial structure, we propose a **cross-modal re-**

ward model that scores diagram-text alignment between the original diagram paired with a generated auxiliary-line description and a reference diagram annotated with the ground-truth auxiliary lines. This reward provides geometry-aware supervision without relying on executable drawing code or precise geometric specifications, enabling robust scaling across diverse diagram styles. We integrate this cross-modal reward, alongside a final-answer reward, into a GRPO-based RL stage to align intermediate constructions with the diagram while maintaining final-answer accuracy. An overview of the stage is illustrated in Figure 2.

2.4.1 Cross-modal Reward Model

Given an original diagram I , a textual description of auxiliary lines d (either the ground-truth description d_{aux} or a perturbed variant d_{aux}^-), and a reference diagram I^+ annotated with the ground-truth auxiliary lines, the reward model evaluates the geometric relations implied by applying d to I against the additional geometric structures present in I^+ but absent from I . Rather than relying on surface-level similarity, it assesses diagram-text relational consistency by verifying whether geometric relations specified in d , such as parallelism, orthogonality, and angle bisection, are satisfied in the reference diagram I^+ . Accordingly, the proposed reward exhibits three desirable properties: (1) **Cross-modal relational alignment**, which evaluates diagram-text consistency at the level of geometric relations rather than surface-level or lexical similarity; (2) **Render-free and coordinate-free**, as it avoids dependence on executable drawing code or pixel-accurate coordinates, relying instead on relational correspondence between diagrams and textual descriptions; and (3) **Fine-grained supervision**, assigning intermediate scores to partially correct yet geometrically meaningful constructions, thereby enabling precise credit assignment in multi-step reasoning. In summary, the cross-modal reward evaluates diagram-text spatial consistency at the level of geometric relations, assessing whether and to what extent the generated auxiliary lines align with the intended geometric structure, without relying on executable rendering code methods. Next, we describe how to automatically **construct diagram-text supervision** at scale and use it to **train the cross-modal reward model**.

Constructing Diagram-Text Supervision. Each training example is represented as $\langle I, d, I^+, \hat{y} \rangle$, where $\hat{y} = (r, s)$ contains a brief justification r and

a consistency score $s \in [0, 1]$ indicating how well d aligns with I^+ given I . We construct this supervision dataset via a fully automated pipeline (see Figure 2). Starting from high-quality supervision triplets $\langle I, d_{\text{aux}}, I^+ \rangle$ constructed as described in Section 3, we systematically generate challenging negative descriptions to support robust diagram-text supervision. Specifically, we design a set of rule-based perturbation templates that simulate common auxiliary-line construction errors, including *partial deletion*, *intersection alteration*, *incorrect line connections*, *adding irrelevant lines*, *unrelated auxiliary lines*. Building on these templates, we further leverage a large language model to synthesize diverse and linguistically varied negative descriptions d_{aux}^- . These negatives are lexically fluent and semantically plausible, yet geometrically inconsistent with the intended construction encoded in the reference diagram I^+ , thereby providing hard counterexamples beyond surface-level mismatches. To assess the consistency between each description $d \in \{d_{\text{aux}}, d_{\text{aux}}^-\}$ and the target construction I^+ , we adopt an *LVLM-as-a-Judge* strategy. Concretely, the LVLM is prompted to evaluate diagram-text alignment by comparing the original diagram paired with the description $\langle I, d \rangle$ against the reference diagram I^+ , and to produce both a natural-language rationale r and a scalar alignment score $s \in [0, 1]$. This automated evaluation yields interpretable explanations alongside valued supervision signals, enabling scalable and fine-grained diagram-text supervision that spans faithful auxiliary-line descriptions as well as adversarially perturbed constructions.

Training Cross-Modal Reward Model. Given the input triplet $\langle I, d, I^+ \rangle$, the model outputs a structured prediction $\hat{y} = (r, s)$. We train the model by maximizing the conditional likelihood of the serialized output:

$$p_\phi(\hat{y} | I, d, I^+) = \prod_{i=1}^T p_\phi(\hat{y}_i | I, d, I^+, \hat{y}_{<i}) \quad (1)$$

where T denotes the length of the generated sequence \hat{y} , \hat{y}_i is the i -th token in the output, and $\hat{y}_{<i}$ represents the sequence of previously generated tokens. The consistency score is indicated as $r_{\text{aux}} = s = \text{Score}(\hat{y})$, where higher values correspond to better consistency.

Through this training, we obtain a reward model that provides precise feedback on diagram-text alignment between auxiliary-line descriptions and the reference diagram. This model serves as a key

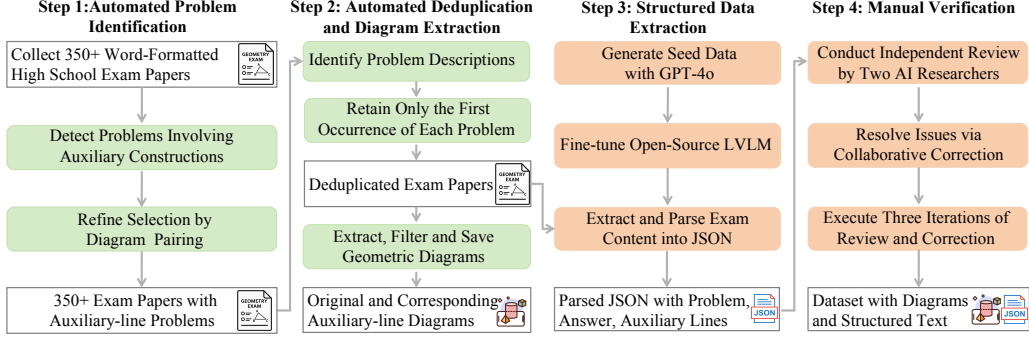


Figure 3: Overview of the proposed data creation pipeline.

component of our framework, guiding the policy toward auxiliary-line constructions that are geometrically consistent and diagram-grounded.

2.4.2 Optimization

We adopt GRPO as the policy optimization algorithm. The overall reward signal combines the cross-modal reward with a final-answer reward defined as a binary score, yielding 1 if the predicted final answer matches the ground truth and 0 otherwise, *i.e.*, $r = \alpha r_{\text{aux}} + (1 - \alpha)r_{\text{ans}}$.

Given a geometric diagram I and a question q , GRPO samples a set of response sequences $\{y_1, y_2, \dots, y_G\}$ from the old policy $\pi_{\theta_{\text{old}}}$. The policy π_{θ} is then optimized by maximizing the following objective:

$$\mathcal{L}_{\text{GRPO}} = \frac{1}{G} \sum_{i=1}^G \left(\min \left(\frac{\pi_{\theta}(y_i \mid I, q)}{\pi_{\theta_{\text{old}}}(y_i \mid I, q)} A_i, \text{clip} \left(\frac{\pi_{\theta}(y_i \mid I, q)}{\pi_{\theta_{\text{old}}}(y_i \mid I, q)}, 1 - \epsilon, 1 + \epsilon \right) A_i \right) - \beta \mathbb{D}_{\text{KL}}(\pi_{\theta} \parallel \pi_{\text{ref}}) \right) \quad (2)$$

Here, G denotes the group size, while ϵ and β are hyperparameters for clipping and the KL penalty.

3 Data Creation

We curate the AuxSolidMath dataset to support training and evaluation of auxiliary-line reasoning in solid geometry. As illustrated in Figure 3, our data creation pipeline proceeds through four progressive steps: **automated problem identification, automated deduplication and diagram extraction, structured data extraction, and manual verification**. The pipeline standardizes raw exam problems into semantically aligned, high-quality multimodal instances that support training vision-language models for auxiliary-line geometric reasoning (More details in Appendix B). Figure 4 shows an example from the dataset. Each instance is represented as a five-tuple consisting of the *problem description*, the *final answer*, the *auxiliary-line description*, the *original diagram*, and the *auxiliary-line diagram*.

Automated Problem Identification. We curate AuxSolidMath from over 350 authentic high-school geometry exam sets using a two-stage filter that selects problems explicitly requiring auxiliary-line constructions, based on cue-verb retrieval from reference solutions and verification of paired original and auxiliary-line-annotated diagrams.

Automated Deduplication and Diagram Extraction. We automatically deduplicate the dataset and extract paired diagrams to ensure unique and high-quality instances. Duplicates are detected by textual matching, and only the first occurrence is retained. For each retained problem, we extract the original and auxiliary-line-annotated diagrams and apply OpenCV-based filtering to discard low-resolution or unclear images.

Structured Data Extraction. Building on the high-quality diagram pairs obtained in the previous step, we extract three textual fields for each problem: the problem description, the final answer, and the auxiliary-line description. Because the source Word files embed MathType formulas that standard parsers handle poorly, we render pages as images and parse them with a fine-tuned LVLM. All outputs are packaged in a structured JSON format.

Manual Verification. Each instance is independently reviewed by two AI researchers to ensure accuracy, completeness, uniqueness, semantic consistency, and visual quality. Instances flagged by either reviewer undergo collaborative re-examination, with up to three review rounds to identify and correct subtle or ambiguous errors. This step resolves complex symbolic expressions and diagrammatic ambiguities that automated tools often misinterpret, and remains indispensable for ensuring high data fidelity in model training and evaluation.

Dataset Statistics. AuxSolidMath comprises 3,018 solid geometry problems collected from real high school examination papers. Within

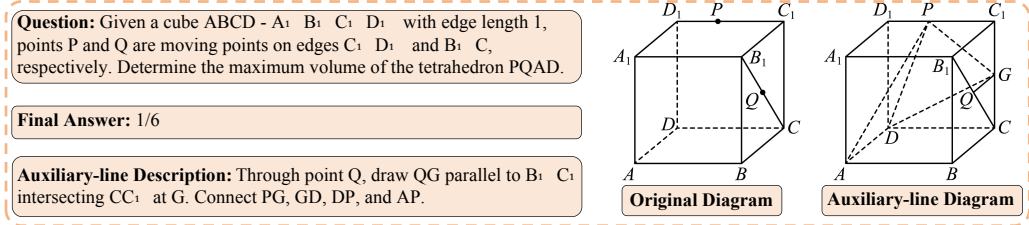


Figure 4: An example from the AuxSolidMath dataset.

this dataset, we curate a new benchmark, GeoAuxBench, designed specifically to evaluate a model’s ability to construct auxiliary lines, a skill essential to solving complex geometry problems. GeoAuxBench contains 302 examples and is divided into two difficulty levels, *Easy* (150) and *Hard* (152), using the original difficulty annotations from the source exam papers rather than post hoc labels. *Hard* problems involve reasoning over implicit spatial relations (e.g., cross-plane or hidden projections), while *Easy* problems rely on explicit relations. By inheriting these exam-defined criteria, GeoAuxBench supports realistic evaluation of auxiliary-line construction in solid geometry.

4 Experiments

4.1 Experimental Settings

Benchmark. We conduct our evaluation on **GeoAuxBench**, a newly introduced benchmark for auxiliary-line construction with two difficulty tiers: **Easy** and **Hard**. We further report results on widely used benchmarks, *i.e.*, **MathVision** (Wang et al., 2024a), **SolidGeo** (Wang et al., 2025a), and the **OlympiadBench** subset of SolidGeo.

Metrics. We evaluate model performance using Pass@k (Chen et al., 2021b), a widely adopted metric introduced by OpenAI. Specifically, we report Pass@1 and Pass@5: Pass@1 measures the accuracy of a single generated solution, while Pass@5 denotes the proportion of problems for which at least one of five generated solutions is correct.

Models. We assess ³ at two model scales, 3B and 7B, both built upon the Qwen2.5-VL backbone. We compare GeoVLM to 20 strong LVLM baselines, covering both closed-source and open-source models, as well as representative methods following the code-driven visual construction paradigm, including V-Thinker (Qiao et al., 2025) and CodePlot-CoT (Duan et al., 2025).

³The code will be publicly available soon at <https://github.com/PersistenceForever/GeoVLM>

4.2 Main Results

As shown in Table 1 and Table 2, we make three key observations: **(1) GeoVLM-
Math achieves strong and robust performance among models of comparable scale across benchmarks.** On GeoAuxBench, both GeoVLM-3B and GeoVLM-7B outperform their corresponding base models, Qwen2.5-VL-3B-Instruct and Qwen2.5-VL-7B-Instruct, on pass@5. GeoVLM-3B improves by **+3.53%** (11.59% \rightarrow 15.12%), while GeoVLM-7B yields a larger gain of **+10.16%** (15.89% \rightarrow 26.05%). Moreover, GeoVLM consistently surpasses the representative code-driven visual construction method V-Thinker on Pass@5, improving by **+12.14%** (13.91% \rightarrow 26.05%), despite not relying on executable drawing code or intermediate diagram rendering. Beyond this task-aligned benchmark, GeoVLM also achieves the best performance among the compared models on widely used public benchmarks. These results demonstrate that the auxiliary-line-aware training signal generalizes beyond GeoAuxBench and improves geometric reasoning robustness. **(2) GeoAuxBench-Hard is a challenging benchmark that clearly distinguishes LVLM capabilities in geometric reasoning.** For example, even strong closed-source models such as Gemini-2.5-Flash and gpt-5-mini achieve Pass@1 scores of **63.16%**, whereas Qwen2.5-VL-7B-Instruct attains only **13.16%**, highlighting a substantial performance gap. This is primarily because the benchmark demands deliberate auxiliary-line construction and multi-step spatial reasoning while minimizing shortcut opportunities, and provides reference diagrams for fine-grained error analysis. Together, GeoAuxBench-Hard serves as a concise yet highly discriminative testbed for differentiating LVLM capabilities. **(3) Model scale alone does not compensate for insufficient auxiliary-line awareness.** On GeoAuxBench-Easy, GeoVLM-7B achieves higher pass@5 than Qwen2.5-VL-32B-Instruct (**35.56%** vs. **23.33%**). On GeoAuxBench-Hard,

LVLM	Easy		Hard		Average	
	Pass@1	Pass@5	Pass@1	Pass@5	Pass@1	Pass@5
Closed-source LVLMs						
gpt-5-mini	89.33	92.67	63.16	75.00	76.16	83.78
o4-mini-2025-04-16	84.00	93.33	60.53	74.34	72.19	83.77
GPT-4o	8.67	25.33	6.58	15.13	7.62	20.20
Gemini-2.0-Flash	37.33	62.67	25.00	39.47	31.12	50.99
Gemini-2.5-Flash	84.00	91.33	63.16	78.95	73.51	85.10
Claude 3.7 Sonnet 20250219	15.33	41.33	13.16	28.29	14.24	34.77
Claude Sonnet 4 20250514	56.00	77.33	30.92	44.74	43.38	60.93
Open-source LVLMs (3B-14B)						
V-Thinker (7B)	8.00	17.33	3.29	10.53	5.63	13.91
InternVL3-8B	9.33	25.33	5.92	15.79	7.61	20.53
Llama-3.2-11B-Vision-Instruct	2.00	12.00	3.29	5.92	2.65	8.94
InternVL3-14B	13.33	28.67	5.92	15.13	9.60	21.86
Qwen2.5-VL-3B-Instruct	2.00	14.89	1.97	8.33	1.98	11.59
GeoVLM-3B (Ours)	12.89	20.44	5.70	9.87	9.27	15.12
Qwen2.5-VL-7B-Instruct	5.14	20.67	3.95	11.18	4.54	15.89
GeoVLM-7B (Ours)	14.67	35.56	5.92	16.67	10.27	26.05
Open-source LVLMs (17B-78B)						
CodePlot-CoT (32B)	4.00	8.67	2.63	5.26	3.31	6.95
Qwen2-VL-72B-Instruct	6.00	15.33	5.26	8.55	5.63	11.92
Qwen2.5-VL-32B-Instruct	20.67	23.33	11.18	13.16	15.89	18.21
Llama-4-Scout-17B-16E-Instruct	20.67	36.67	7.89	18.42	14.24	27.48
InternVL3-38B	19.33	41.33	10.53	21.71	14.90	31.46
Qwen2.5-VL-72B-Instruct	24.00	40.67	13.16	19.74	18.54	30.14
InternVL3-78B	16.67	36.67	9.21	21.05	12.92	28.81

* Bold indicates the best results for models of similar sizes.

Table 1: Overall evaluation on GeoAuxBench (%).

LVLM	MathVision		OlympiadBench		SolidGeo	
	Pass@1	Pass@5	Pass@1	Pass@5	Pass@1	Pass@5
V-Thinker (7B)	16.36	31.82	4.60	13.22	10.39	29.38
CodePlot-CoT (32B)	10.00	29.09	2.87	5.17	16.62	30.86
Qwen2.5-VL-3B-Instruct	5.45	16.36	2.30	6.32	5.04	12.17
GeoVLM-3B (Ours)	5.45	20.91	14.94	25.86	14.54	32.34
Qwen2.5-VL-7B-Instruct	11.82	20.91	2.87	13.22	5.34	14.84
GeoVLM-7B (Ours)	16.36	36.36	25.86	50.57	17.51	42.34

Table 2: Overall evaluation on widely used benchmarks (%).

GeoVLM-7B also outperforms Qwen2.5-VL-32B-Instruct (**16.67%** vs. **13.16%**). Error analysis shows that Qwen2.5-VL-32B-Instruct rarely constructs auxiliary lines and thus overlooks latent spatial constraints, whereas GeoVLM-7B proactively introduces appropriate auxiliary lines and exploits the induced constraints during reasoning. This comparison highlights that auxiliary-line supervision, rather than model scale alone, is critical for reliable geometric reasoning.

4.3 Cross-modal Reward Model

Leveraging AuxSolidMath triplets $\langle I, d_{\text{aux}}, I^+ \rangle$, we apply rule-based perturbations to simulate typical auxiliary-line errors and use the resulting data to train a cross-modal reward model on Qwen2.5-VL-7B. The dataset comprises 2,970 training examples and 330 test examples. We train the model for 3 epochs with a batch size of 16, using the AdamW optimizer with a learning rate of $2e-5$ and a cosine learning rate scheduler with a 0.1 warm-up ratio. During training, the vision tower and projection

modules are frozen, while the language model remains trainable. The model achieves a pass@1 accuracy of **98.18%** on the test set, indicating reliable alignment between textual auxiliary-line descriptions and their visually annotated counterparts.

4.4 Ablation Studies

Cross-Modal Reward. We assess the role of cross-modal supervision with two variants, keeping all other settings unchanged. (a) *w/o cross-modal reward*. This variant removes all supervision related to auxiliary lines and trains the model solely for final-answer accuracy, with no supervision on whether auxiliary lines are introduced. This allows us to assess the effect of training with answer-only supervision, approximating a setting where auxiliary lines are omitted from the training objective. (b) *Textual reward*. In this variant, cross-modal consistency is replaced with a text-only semantic similarity objective that evaluates the similarity between the generated auxiliary-line description and the ground-truth annotation.

	Easy		Hard		Average	
	Pass@1	Pass@5	Pass@1	Pass@5	Pass@1	Pass@5
GeoVLMath-7B	14.67	35.56	5.92	16.67	10.27	26.05
w/o Cross-Modal Reward	10.89 _{↓3.78}	32.22 _{↓3.34}	4.82 _{↓1.10}	13.60 _{↓3.07}	7.83 _{↓2.44}	22.85 _{↓3.20}
Textual Reward	10.67 _{↓4.00}	28.44 _{↓7.12}	4.39 _{↓1.53}	12.50 _{↓4.17}	7.51 _{↓2.76}	20.42 _{↓5.63}
w/o RL	3.33 _{↓11.34}	20.44 _{↓15.12}	3.95 _{↓1.97}	11.18 _{↓5.49}	3.64 _{↓6.63}	15.78 _{↓10.27}

Table 3: Results of ablation studies (%).

Concretely, we use *EmbeddingGemma* (DeepMind, 2025c) to encode sentences and compute a similarity score for training. This variant favors fluent textual descriptions but does not enforce grounding to the input diagram. *Findings*. As reported in Table 3, removing the cross-modal reward results in performance degradation (Average pass@1: **10.27** → **7.83**, pass@5: **26.05** → **22.85**), underscoring the importance of geometry-aware supervision for instances that require introducing auxiliary lines. Substituting it with a purely textual similarity objective performs even worse (Average pass@1: **10.27** → **7.51**, pass@5: **26.05** → **20.42**), consistent with our pilot finding in Section 1 that incorrect auxiliary lines can be worse than none. These declines suggest that lexical alignment introduces spurious signals and conflicts with precise diagram grounding, favoring surface-level paraphrases over geometry-aware reasoning. Error analysis reveals distinct failure modes: (a) often ignores auxiliary-line construction and overfits to answer-only cues; (b) produces fluent but visually inconsistent descriptions (e.g., incorrect lines) that fail to constrain diagram-based reasoning. Overall, text-only alignment fails to faithfully capture geometric structure, motivating the need for visually grounded, structure-preserving diagram-text alignment to support rigorous verification of geometric measurements and structural relations.

Reinforcement Learning. To quantify the contribution of reinforcement learning, we remove the RL stage and train an SFT-only variant. As shown in Table 3, GeoVLMath-7B trained with SFT+RL consistently outperforms its SFT-only counterpart, with clear performance degradation when the RL stage is removed. This improvement reflects the role of RL in moving beyond strict imitation: reward-aligned optimization encourages exploration of more effective strategies and enables credit assignment for beneficial intermediate steps, rather than relying on surface-level matching alone. As a result, RL acts as a post-SFT catalyst that consolidates preliminary SFT competence into robust multi-step reasoning, particularly in scenarios

requiring auxiliary-line construction.

5 Related Work

Recent LVLMs (Anthropic, 2025b; DeepMind, 2025a; OpenAI, 2025) have advanced geometric problem solving, particularly in plane geometry. Prior work mainly follows two lines: direct generation of answers or reasoning paths from multimodal inputs (Ning et al., 2025; Xia et al., 2025; Gao et al., 2025), which is constrained by intrinsic reasoning capacity, and tool-augmented reasoning that generates executable code for symbolic computation or geometric operations (Zhao et al., 2025; Sharma et al., 2025; Chen et al., 2024). More recently, a code-driven visual construction paradigm has emerged, where models generate code to construct or modify diagrams during reasoning, as exemplified by Visual Sketchpad (Hu et al., 2024), V-Thinker (Qiao et al., 2025), and CodePlot-CoT (Duan et al., 2025). While these methods enable interactive visual feedback, they depend on precise code execution and explicit coordinate annotations, and tightly couple auxiliary-line construction with the LVLM’s intrinsic reasoning, thereby limiting robustness in solid geometry. In contrast, our approach incorporates auxiliary-line construction into an RL framework guided by a cross-modal reward model, decoupling construction quality from intrinsic reasoning, without explicit geometric specifications, enabling robust auxiliary-line reasoning across model scales.

6 Conclusion

Auxiliary-line reasoning in solid geometry exposes a key limitation of current LVLMs: the lack of reliable learning signals for structured visual construction. We address this challenge by formulating auxiliary-line construction as a vision-language alignment problem and introducing a RL framework guided by a cross-modal reward that directly measures diagram-text correspondence. This design enables stable optimization without relying on explicit geometric specifications or executable code. To support learning at scale, we automat-

ically construct **AuxSolidMath**, a high-quality dataset of real-exam solid geometry problems with aligned diagrams and auxiliary-line annotations, providing a reusable resource for the community. Leveraging this framework, **GeoVLMath** consistently improves auxiliary-line reasoning.

Limitations

While our approach demonstrates strong effectiveness for auxiliary-line reasoning in solid geometry, our experiments primarily consider settings where auxiliary-line constructions admit concise high-level descriptions. Extending the evaluation to even broader or more diverse geometric constructions remains an interesting direction for future work. In addition, our cross-modal reward model relies on annotated auxiliary-line diagrams for supervision during reinforcement learning. Although we introduce AuxSolidMath to support this setting, exploring more scalable forms of weak or self-supervised reward signals is a promising direction for future research.

References

- Anthropic. 2025a. Claude 3.7 sonnet and claude code. <https://www.anthropic.com/news/clause-3-7-sonnet>.
- Anthropic. 2025b. Claude 4. <https://www.anthropic.com/news/clause-4>.
- Shuai Bai, Keqin Chen, Xuejing Liu, Jialin Wang, Wenbin Ge, Sibo Song, Kai Dang, Peng Wang, Shijie Wang, Jun Tang, Humen Zhong, Yuanzhi Zhu, Ming-Hsuan Yang, Zhaohai Li, Jianqiang Wan, Pengfei Wang, Wei Ding, Zheren Fu, Yiheng Xu, and 8 others. 2025. Qwen2.5-v1 technical report. *CoRR*, abs/2502.13923.
- Jiaqi Chen, Tong Li, Jinghui Qin, Pan Lu, Liang Lin, Chongyu Chen, and Xiaodan Liang. 2022. Unigeo: Unifying geometry logical reasoning via reformulating mathematical expression. In *Proceedings of the 2022 Conference on Empirical Methods in Natural Language Processing, EMNLP 2022*, pages 3313–3323.
- Jiaqi Chen, Jianheng Tang, Jinghui Qin, Xiaodan Liang, Lingbo Liu, Eric P. Xing, and Liang Lin. 2021a. Geoqa: A geometric question answering benchmark towards multimodal numerical reasoning. In *Findings of the Association for Computational Linguistics: ACL/IJCNLP 2021*, pages 513–523.
- Jingchang Chen, Hongxuan Tang, Zheng Chu, Qianglong Chen, Zekun Wang, Ming Liu, and Bing Qin. 2024. Divide-and-conquer meets consensus: Unleashing the power of functions in code generation. In *Advances in Neural Information Processing Systems 38: Annual Conference on Neural Information Processing Systems 2024, NeurIPS 2024*, Vancouver.
- Mark Chen, Jerry Tworek, Heewoo Jun, Qiming Yuan, Henrique Pondé de Oliveira Pinto, Jared Kaplan, Harri Edwards, Yuri Burda, Nicholas Joseph, Greg Brockman, Alex Ray, Raul Puri, Gretchen Krueger, Michael Petrov, Heidy Khlaaf, Girish Sastry, Pamela Mishkin, Brooke Chan, Scott Gray, and 39 others. 2021b. Evaluating large language models trained on code. *CoRR*, abs/2107.03374.
- DeepMind. 2025a. Gemini 2.5 flash. <https://deepmind.google/models/gemini/flash/>.
- DeepMind. 2025b. Gemini 2.5 pro. <https://deepmind.google/models/gemini/pro/>.
- Google DeepMind. 2025c. Embeddinggemma: A 308m multilingual text embedding model. <https://ai.google.dev/gemma/docs/embeddinggemma?hl=zh-cn>.
- Chengqi Duan, Kaiyue Sun, Rongyao Fang, Manyuan Zhang, Yan Feng, Ying Luo, Yufang Liu, Ke Wang, Peng Pei, Xunliang Cai, Hongsheng Li, Yi Ma, and Xihui Liu. 2025. Codeplot-cot: Mathematical visual reasoning by thinking with code-driven images. *CoRR*, abs/2510.11718.
- Yumeng Fu, Jiayin Zhu, Lingling Zhang, Bo Zhao, Shaoxuan Ma, Yushun Zhang, Yanrui Wu, and Wenjun Wu. 2025. Geolaux: A benchmark for evaluating mllms’ geometry performance on long-step problems requiring auxiliary lines. *CoRR*, arXiv:2508.06226v1.
- Jiahui Gao, Renjie Pi, Jipeng Zhang, Jiacheng Ye, Wan-jun Zhong, Yufei Wang, Lanqing Hong, Jianhua Han, Hang Xu, Zhenguo Li, and Lingpeng Kong. 2025. G-llava: Solving geometric problem with multi-modal large language model. In *The Thirteenth International Conference on Learning Representations, ICLR 2025*.
- Daya Guo, Dejian Yang, Haowei Zhang, Junxiao Song, Ruoyu Zhang, Runxin Xu, Qihao Zhu, Shiron Ma, Peiyi Wang, Xiao Bi, and 1 others. 2025. Deepseek-r1: Incentivizing reasoning capability in llms via reinforcement learning. *arXiv preprint arXiv:2501.12948*.
- Yushi Hu, Weijia Shi, Xingyu Fu, Dan Roth, Mari Ostendorf, Luke Zettlemoyer, Noah A. Smith, and Ranjay Krishna. 2024. Visual sketchpad: Sketching as a visual chain of thought for multimodal language models. In *Advances in Neural Information Processing Systems 38: Annual Conference on Neural Information Processing Systems 2024, NeurIPS 2024, Vancouver*.
- Aaron Hurst, Adam Lerer, Adam P. Goucher, Adam Perelman, Aditya Ramesh, Aidan Clark, AJ Ostrow, Akila Welihinda, Alan Hayes, Alec Radford, Aleksander Madry, Alex Baker-Whitcomb, Alex Beutel,

- Alex Borzunov, Alex Carney, Alex Chow, Alex Kirillov, Alex Nichol, Alex Paino, and 79 others. 2024. Gpt-4o system card. *CoRR*, abs/2410.21276.
- Pan Lu, Hritik Bansal, Tony Xia, Jiacheng Liu, Chunyuan Li, Hannaneh Hajishirzi, Hao Cheng, Kai-Wei Chang, Michel Galley, and Jianfeng Gao. 2024. Mathvista: Evaluating mathematical reasoning of foundation models in visual contexts. In *The Twelfth International Conference on Learning Representations, ICLR 2024*.
- Pan Lu, Ran Gong, Shibiao Jiang, Liang Qiu, Siyuan Huang, Xiaodan Liang, and Song-Chun Zhu. 2021. Inter-gps: Interpretable geometry problem solving with formal language and symbolic reasoning. In *Proceedings of the 59th Annual Meeting of the Association for Computational Linguistics and the 11th International Joint Conference on Natural Language Processing, ACL/IJCNLP 2021*, pages 6774–6786.
- Bin Ma, Pengpeng Jian, Cong Pan, Yanli Wang, and Wei Ma. 2024. A geometric neural solving method based on a diagram text information fusion analysis. *Scientific Reports*, 14(1):31906.
- Meta. 2024. Llama 3.2: Revolutionizing edge ai and vision with open, customizable models.
- Meta. 2025. The llama 4 herd: The beginning of a new era of natively multimodal ai innovation. <https://ai.meta.com/blog/llama-4-multimodal-intelligence/>.
- Maizhen Ning, Zihao Zhou, Qiufeng Wang, Xiaowei Huang, and Kaizhu Huang. 2025. GNS: solving plane geometry problems by neural-symbolic reasoning with multi-modal llms. In *AAAI-25, Sponsored by the Association for the Advancement of Artificial Intelligence*, pages 24957–24965.
- OpenAI. 2025. Gpt-5 system card. <https://cdn.openai.com/gpt-5-system-card.pdf>.
- OpenAI. 2025. Openai o3 and o4-mini system card. <https://cdn.openai.com/pdf/2221c875-02dc-4789-800b-e7758f3722c1/o3-and-o4-mini-system-card.pdf>.
- Runqi Qiao, Qiuna Tan, Minghan Yang, Guanting Dong, Peiqing Yang, Shiqiang Lang, Enhui Wan, Xiaowan Wang, Yida Xu, Lan Yang, Chong Sun, Chen Li, and Honggang Zhang. 2025. V-thinker: Interactive thinking with images. *CoRR*, abs/2511.04460.
- Aditya Sharma, Aman Dalmia, Mehran Kazemi, Amal Zouaq, and Christopher Pal. 2025. Geocoder: Solving geometry problems by generating modular code through vision-language models. In *Findings of the Association for Computational Linguistics: NAACL 2025*, pages 7340–7356.
- Ke Wang, Junting Pan, Weikang Shi, Zimu Lu, Houxing Ren, Aojun Zhou, Mingjie Zhan, and Hongsheng Li. 2024a. Measuring multimodal mathematical reasoning with math-vision dataset. In *Advances in Neural Information Processing Systems 38: Annual Conference on Neural Information Processing Systems 2024, NeurIPS 2024*.
- Peijie Wang, Chao Yang, Zhong-Zhi Li, Fei Yin, Dekang Ran, Mi Tian, Zhilong Ji, Jinfeng Bai, and Chenglin Liu. 2025a. SOLIDGEO: measuring multimodal spatial math reasoning in solid geometry. *CoRR*, abs/2505.21177.
- Peng Wang, Shuai Bai, Sinan Tan, Shijie Wang, Zhihao Fan, Jinze Bai, Keqin Chen, Xuejing Liu, Jialin Wang, Wenbin Ge, Yang Fan, Kai Dang, Mengfei Du, Xuancheng Ren, Rui Men, Dayiheng Liu, Chang Zhou, Jingren Zhou, and Junyang Lin. 2024b. Qwen2-vl: Enhancing vision-language model’s perception of the world at any resolution. *CoRR*, abs/2409.12191.
- Xiaofeng Wang, Yiming Wang, Wenhong Zhu, and Rui Wang. 2025b. Do large language models truly understand geometric structures? In *The Thirteenth International Conference on Learning Representations, ICLR 2025*.
- Haoran Wei, Yaofeng Sun, and Yukun Li. 2025. Deepseek-ocr: Contexts optical compression. *arXiv preprint arXiv:2510.18234*.
- Renqiu Xia, Mingsheng Li, Hancheng Ye, Wenjie Wu, Hongbin Zhou, Jiakang Yuan, Tianshuo Peng, Xinyu Cai, Xiangchao Yan, Bin Wang, Conghui He, Botian Shi, Tao Chen, Junchi Yan, and Bo Zhang. 2025. Geox: Geometric problem solving through unified formalized vision-language pre-training. In *The Thirteenth International Conference on Learning Representations, ICLR 2025*.
- Shicheng Xu, Liang Pang, Huawei Shen, Xueqi Cheng, and Tat-Seng Chua. 2024. Search-in-the-chain: Interactively enhancing large language models with search for knowledge-intensive tasks. In *Proceedings of the ACM on Web Conference 2024, WWW 2024*, pages 1362–1373.
- Bohan Zhang, Xiaokang Zhang, Jing Zhang, Jifan Yu, Sijia Luo, and Jie Tang. 2025. Cot-based synthesizer: Enhancing LLM performance through answer synthesis. In *Proceedings of the 63rd Annual Meeting of the Association for Computational Linguistics (Volume 1: Long Papers), ACL 2025*, pages 6286–6303.
- Renrui Zhang, Dongzhi Jiang, Yichi Zhang, Haokun Lin, Ziyu Guo, Pengshuo Qiu, Aojun Zhou, Pan Lu, Kai-Wei Chang, Yu Qiao, Peng Gao, and Hongsheng Li. 2024. MATHVERSE: does your multi-modal LLM truly see the diagrams in visual math problems? In *Computer Vision - ECCV 2024 - 18th European Conference*, pages 169–186.
- Junbo Zhao, Ting Zhang, Jiayu Sun, Mi Tian, and Hua Huang. 2025. Pi-gps: Enhancing geometry problem solving by unleashing the power of diagrammatic information. *CoRR*, abs/2503.05543.

Yaowei Zheng, Richong Zhang, Junhao Zhang, Yanhan Ye, Zheyuan Luo, and Yongqiang Ma. 2024. Llamafactory: Unified efficient fine-tuning of 100+ language models. *CoRR*, abs/2403.13372.

Jinguo Zhu, Weiyun Wang, Zhe Chen, Zhaoyang Liu, Shenglong Ye, Lixin Gu, Hao Tian, Yuchen Duan, Weijie Su, Jie Shao, Zhangwei Gao, Erfei Cui, Xue-hui Wang, Yue Cao, Yangzhou Liu, Xingguang Wei, Hongjie Zhang, Haomin Wang, Weiye Xu, and 32 others. 2025. Internvl3: Exploring advanced training and test-time recipes for open-source multimodal models. *CoRR*, abs/2504.10479.

A The Use of AI Assistants

In this paper, ChatGPT was used exclusively for language polishing, including grammar correction, phrasing, and stylistic refinement. It was not used to generate scientific content such as research ideas, methods, experiments, or related work. No confidential, personal, or proprietary information was shared with the model. The authors take full responsibility for the scientific content, which was entirely authored and verified by the authors.

B Data Creation

In this section, we detail the four progressive steps of our data creation pipeline.

B.1 Automated Problem Identification

To construct the AuxSolidMath dataset, we first collect over 350 sets of high school geometry problems from publicly available online sources. Given that the dataset is intended to support constructive geometric reasoning, we specifically target problems that necessitate auxiliary line constructions as integral components of their solutions.

To efficiently identify such problems, we design an automated two-stage filtering pipeline using Python scripts. In the first stage, we detect problems whose solutions contain explicit mentions of auxiliary-line constructions. Specifically, we apply regular expression patterns to locate question number markers that are explicitly present in the exam papers and use these markers to segment the content into individual problem units. For each problem, we examine the solution for verbs that signal the introduction of auxiliary lines (e.g., "connect," "construct," "draw," "establish"). Problems lacking such terms are discarded, while those containing relevant cues are retained. In the second stage, we further refine the selection by ensuring that each retained problem contains both the original diagram and an auxiliary-line diagram. To this

end, we quantify the number of diagrams associated with each problem. Problems with fewer than two diagrams are excluded, whereas those with at least two, which usually represent the original and modified diagrams, are preserved. This automated pipeline enables scalable and consistent filtering of auxiliary-line geometry problems, significantly reducing manual annotation effort.

B.2 Automated Deduplication and Diagram Extraction

Upon identifying geometry problems requiring auxiliary lines, we employ an automated pipeline to deduplicate instances and extract the associated diagrams. This step guarantees the uniqueness and visual quality of data instances for downstream model training.

Problem Deduplication. To eliminate duplicate problems, we retain only the first occurrence of each unique problem based on its textual content. Concretely, we initialize a global problem set as an empty collection. We then sequentially process all Word-formatted exam papers, examining only the problem descriptions while ignoring the associated solutions and diagrams. For each problem, if its description is not already present in the global set, we add the problem; otherwise, we discard it as a duplicate. This procedure ensures that identical problems, which often recur across different examinations, are retained only once.

Diagram Extraction. Following deduplication, we extract, filter, and store the geometric diagrams associated with each retained problem. A key challenge lies in reliably distinguishing true geometric figures from image-embedded mathematical expressions (e.g., MathType equations), as both appear in Word exam papers. Existing Python libraries are unable to make this distinction accurately, often misclassifying equations as diagrams and introducing significant noise into the extraction process. To overcome this limitation, we innovatively integrate the Apache POI library through a custom Java implementation, enabling fine-grained control over the parsing of Word documents. This setup enables reliable identification and extraction of genuine geometric diagrams while effectively filtering out formula-rendered images. To further ensure visual quality, the extracted diagrams are then processed using OpenCV to discard low-resolution or unclear diagrams. The remaining diagrams are subsequently saved using a standardized naming convention that distinguishes between the original

and the annotated versions of the auxiliary lines. To be more specific, for each problem indexed by i , we store two images: $\{i\}.png$, which contains the original diagram, and $\{i\}_\text{auxiliary}.png$, which includes the corresponding auxiliary-line diagram. This consistent format facilitates downstream alignment between textual and visual modalities within the multimodal processing pipeline.

B.3 Structured Data Extraction

Building on the high-quality geometric diagrams obtained in the previous step, we proceed to extract the corresponding textual content for each instance, including the problem description, the final answer, and the auxiliary-line description. This extraction process is non-trivial, as the original Word documents frequently embed mathematical expressions in MathType formats that are not reliably supported by standard document parsing tools.

To address this challenge, we render the processed Word documents as images, thereby enabling LVLMs to leverage their visual reasoning capabilities. Although this approach appears straightforward, open-source models such as Qwen2.5-VL-7B-Instruct (Bai et al., 2025) often struggle to accurately parse complex geometry problems involving symbolic notation and mathematical expressions. In contrast, closed-source models like GPT-4o (Hurst et al., 2024) exhibit significantly stronger performance, but their reliance on commercial APIs introduces substantial costs and limits scalability in large-scale applications. To balance accuracy with scalability, we adopt a hybrid strategy⁴. Specifically, we first utilize an advanced closed-source model (*i.e.*, GPT-4o) to generate a small, high-quality seed dataset comprising 300 manually verified instances. This curated dataset is then used to fine-tune an LVLM (*i.e.*, Qwen2.5-VL-7B-Instruct), resulting in a lightweight, domain-adapted model capable of accurate and scalable text extraction. The final output consists of the extracted problem description, the final answer, and the auxiliary-line description, all encapsulated in a structured JSON format. This unified representation facilitates consistent data handling and serves as a foundation for training a robust open-source text extraction model. By releasing this model, we aim to contribute a practical and reusable re-

source to the broader research community working on geometry-aware vision-language understanding.

B.4 Manual Verification

To ensure the quality and reliability of the final dataset, we perform a manual verification step that assesses each data instance in terms of accuracy, completeness, uniqueness, and semantic consistency, alongside visual quality criteria such as image clarity and resolution. Two AI researchers serve as independent checkers. Each instance is independently reviewed by both researchers. If either checker identifies a potential issue, the instance is collaboratively revised. This process is repeated up to three times per instance, ensuring that all errors, including subtle or ambiguous ones, are systematically identified and corrected. Manual verification plays a critical role in resolving complex symbolic expressions and ambiguous diagrammatic content that automated tools may misinterpret. Despite its relatively low cost and effort, this step remains indispensable for ensuring the high data fidelity necessary for a reliable model.

C Experimental Setup

C.1 Models

On the closed-source models, we include leading models such as gpt-5-mini (OpenAI, 2025), o4-mini (OpenAI, 2025) and GPT-4o (Hurst et al., 2024), Gemini-2.0-Flash and Gemini-2.5-Flash (DeepMind, 2025a), Claude 3.7 Sonnet (Anthropic, 2025a) and Claude Sonnet 4 20250514 (Anthropic, 2025b). These models represent the forefront of multimodal reasoning among closed-source models, although their internal architectures remain undisclosed. On the open-source models, we consider several publicly available high-performance models, including the Qwen2 VL (Wang et al., 2024b) and Qwen2.5 VL series (Bai et al., 2025), InternVL 3 families (Zhu et al., 2025), LLaMA-3.2-11B-Vision-Instruct (Meta, 2024) and Llama-4-Scout-17B-16E-Instruct (Meta, 2025). In addition, we include representative methods following the code-driven visual construction paradigm, namely V-Thinker (Qiao et al., 2025) and CodePlot-CoT (Duan et al., 2025), which generate executable code to construct or modify diagrams as part of the reasoning process. These approaches provide an important comparison point for evaluating different strategies of integrating visual construction into

⁴DeepSeek-OCR(Wei et al., 2025) was released on October 20, 2025 and was not available during data construction. A Qwen2.5-VL-based extractor fine-tuned on 300 seed samples achieved approximately 98% accuracy and was therefore used.

multimodal reasoning. Together, these models encompass a range of design paradigms, parameter scales, and instruction tuning strategies, forming a comprehensive and robust foundation for evaluating auxiliary-line reasoning in multimodal settings. Note that models such as Gemini-2.5 Pro (DeepMind, 2025b) and OpenAI o3 (OpenAI, 2025) are excluded from our study due to limited accessibility and high inference costs.

C.2 Training Implementation Details

We adopt a two-stage training paradigm based on the Qwen2.5-VL series, including Qwen2.5-VL-3B and Qwen2.5-VL-7B, consisting of the SFT stage and the RL stage.

SFT Stage. The SFT phase is conducted using the LLaMA-Factory framework (Zheng et al., 2024). For Qwen2.5-VL-7B, we train the model for 5 epochs with a per-device batch size of 2 and a gradient accumulation step of 8 (effective batch size of 16). We use the AdamW optimizer with a learning rate of 2e-5 and apply a cosine learning rate scheduler with a warmup ratio of 0.1. The model is trained in bf16 precision. Vision and projection modules are frozen during this stage, while the language model remains unfrozen. For Qwen2.5-VL-3B, we adopt the same training configuration as the 7B variant, except learning rate and training epochs. Specifically, Qwen2.5-VL-3B is trained for 5 epochs with a learning rate of 3e-5.

RL Stage. For the Qwen2.5-VL-7B model, both training and validation data are loaded from Parquet files containing question-diagram pairs. The maximum response length is set to 8,192 tokens, and both the rollout and validation batch sizes are set to 16. The actor is optimized using AdamW (learning rate 2e-6, weight decay 1e-2, no warmup). KL regularization is applied using the `low_var_kl` penalty with a coefficient of 1e-2. Training runs for 6 epochs using bf16 precision, with gradient checkpointing and partial FSDP offloading enabled for memory efficiency.

Rewards. The overall reward is the sum of a cross-modal auxiliary-line consistency reward and a final-answer accuracy reward, where the auxiliary-line component is weighted by $\alpha = 0.1$. For Qwen2.5-VL-3B, we adopt the same RL configuration as the 7B model, with adjustments to the batch size and the number of training epochs. Specifically, Qwen2.5-VL-3B is trained for 4 epochs with a batch size of 8.

All training was conducted on a server equipped

with two NVIDIA A100 80GB and two NVIDIA A800 80GB GPUs. The SFT stage was performed on two A100 GPUs, whereas the reinforcement learning stage utilized all four GPUs. For response generation during training and evaluation, we enabled stochastic sampling with temperature set to 0.7 and top-p set to 0.95.

D Related Work

In this section, we also review benchmarks and datasets for geometric reasoning. Most benchmarks and datasets for geometric problem solving focus on plane geometry, where diagrams and problems involve two-dimensional figures. Well-known resources in this area include Geometry3K (Lu et al., 2021), GeoQA (Chen et al., 2021a), UniGeo (Chen et al., 2022), and GeomRel (Wang et al., 2025b), which primarily cover plane geometry problems. A concurrent benchmark, GeoLaux (Fu et al., 2025), explores the use of auxiliary lines in plane geometry, but is limited to simple cases and lacks engagement with the spatial complexity of solid geometry. Nonetheless, there remains a lack of dedicated resources for solid geometry, even though solving such problems often requires interpreting three-dimensional relationships and drawing auxiliary lines to uncover hidden spatial structures. While SolidGeo (Wang et al., 2025a) is a recent benchmark that focuses exclusively on solid geometry, it does not explicitly require auxiliary lines for solving its problems, leaving this important aspect of spatial reasoning underexplored. Similarly, other benchmarks such as MathVision (Wang et al., 2024a), MathVista (Lu et al., 2024), and MathVerse (Zhang et al., 2024) contain only a limited number of solid geometry problems, and these also do not require auxiliary lines to reach the solution. As a result, these resources fall short of evaluating a model’s ability to solve complex solid geometry problems where auxiliary lines are essential for uncovering implicit spatial relationships. To address this gap, we present AuxSolidMath, the first dedicated dataset for solid geometry problems that require auxiliary lines to solve. It offers comprehensive multimodal supervision, including the original diagram, the problem statement, textual descriptions of the required auxiliary lines, the final answer, and a corresponding diagram annotated with those lines, enabling models to learn how the auxiliary lines facilitate solid geometry reasoning.

SYSTEM_PROMPT_FOR_SUPERVISED_FINE-TUNING

SYSTEM_PROMPT_FOR_SUPERVISED_FINE-TUNING = """

You are a mathematician skilled in solving geometry problems through step-by-step reasoning. Solve the given geometry problem based on a geometric diagram and a natural language question. Use ‘[AUX]...[/AUX]’ to indicate auxiliary constructions, such as establishing coordinate systems or constructing auxiliary lines. Finally, provide your final answer within ‘Final Answer:....’.

"""

USER_PROMPT_FOR_SUPERVISED_FINE-TUNING

USER_PROMPT_FOR_SUPERVISED_FINE-TUNING = """

Image: <image>

Question: {question}

"""

Figure 5: Prompts for supervised fine-tuning.

SYSTEM_PROMPT_FOR_CROSS-MODAL_REWARD_MODEL

SYSTEM_PROMPT_FOR_CROSS-MODAL_REWARD_MODEL = """

You are a professional geometry reasoning evaluator. Your task is to evaluate whether a given textual description of auxiliary lines accurately explains the visual difference between the original diagram and the auxiliary-line diagram.

Score the description on a scale from 0 to 1:

1. 1 indicates a fully accurate and helpful description.
2. 0 indicates a completely irrelevant or misleading description.
3. Intermediate values (e.g., 0.25/ 0.50/ 0.75) reflect partial relevance or minor issues.

Return exactly one line:

<brief justification>. Score: <s>.

"""

USER_PROMPT_FOR_CROSS-MODAL_REWARD_MODEL

USER_PROMPT_FOR_CROSS-MODAL_REWARD_MODEL = """

Image (original diagram): <image I >

Image (auxiliary-line diagram): <image I^+ >

Auxiliary-line description: {generated_aux_description}

"""

Figure 6: Prompts for cross-modal reward model.

E Prompts

E.1 Prompts for Supervised Fine-tuning

Figure 5 presents the two-part prompt template used in our supervised dataset. The system prompt assigns the solver role and enforces formatting: auxiliary lines must be wrapped in [AUX]...[/AUX] and the final answer must appear as plain text in Final Answer:.... The user prompt is multimodal, pairing a diagram referenced by the <image> token with the natural language question {question}, which yields explicit reasoning steps and a final answer.

E.2 Prompts for Cross-Modal Reward Model

Using the prompt as shown in Figure 6, the cross-modal reward model compares the description of the auxiliary line generated by the policy model against a pair of diagrams, the original image I and its auxiliary-line counterpart I^+ , and returns a single line justification and a calibrated score in $[0, 1]$ that measures visual–textual agreement. The instruction emphasizes the correctness of auxiliary-line constructions and adherence to geometric constraints. Higher scores indicate stronger alignment.

F Representative Examples

As illustrated in Figure 7, we present qualitative examples from the AuxSolidMath dataset, including the question, the final answer, the auxiliary-line description, the original diagram, and the auxiliary-line diagram. The examples showcase diverse strategies for constructing auxiliary lines and demonstrate that explicit annotations reveal the key spatial constraints.

G Case Study

G.1 Successful Cases

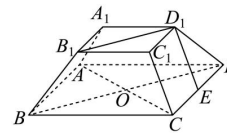
In this section, we present representative cases produced by GeoVLM-7B (see Figure 8). The examples illustrate how valid auxiliary-line constructions capture essential spatial constraints, which in turn lead to correct final answers. Collectively, these results provide concrete evidence of both the effectiveness of our training framework and the model’s capacity to tackle complex geometric reasoning requiring robust visual understanding and precise symbolic inference.

G.2 Failure Cases

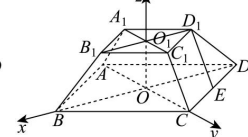
In this section, we illustrate typical failure cases generated by GeoVLM-7B (see Figure 9). The observed failures are exemplified by mis-specified coordinate systems and auxiliary-line descriptions that are irrelevant to the diagram, both of which fail to capture essential spatial constraints and may yield incorrect final answers. To mitigate such errors, we will explore diffusion-based drawing modules that render auxiliary lines directly on the original diagram and support iterative correction as part of future work.

Question: As shown in the diagram, consider the regular truncated quadrilateral pyramid ABCD - A₁ B₁ C₁ D₁. Given that $\angle B_1 BA = 60^\circ$, $AB = 2A_1 B_1 = 4$, and E is the midpoint of segment CD, determine the sine of the angle between line ED₁ and plane ABB₁ A₁.

Final Answer: $\sqrt{6}/3$



Original Diagram

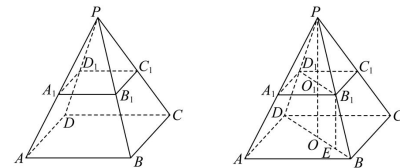


Auxiliary-line Diagram

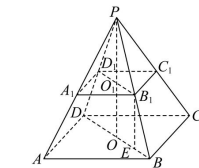
Auxiliary-line Description: Connect A₁ C₁, which intersects B₁ D₁ at O₁, then connect OO₁. Take O as the origin, and let the lines along OB, OC, and OO₁ be the x-axis, y-axis, and z-axis, respectively, then establish the three-dimensional Cartesian coordinate system O-xyz.

Question: As shown in the diagram, consider the regular truncated quadrilateral pyramid ABCD - A₁ B₁ C₁ D₁. The edge lengths of the upper and lower bases are 2 and 3, respectively, and the lateral edge length is $\sqrt{2}$. By extending AA₁, BB₁, CC₁, DD₁, they intersect at point P. Determine the volume of the quadrilateral pyramid P - A₁ B₁ C₁ D₁.

Final Answer: $4\sqrt{6}/3$



Original Diagram

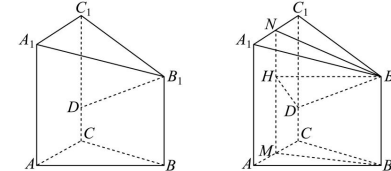


Auxiliary-line Diagram

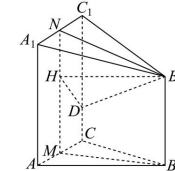
Auxiliary-line Description: Through point P, construct PO perpendicular to the base ABCD at point O, intersecting the plane A₁ B₁ C₁ D₁ at point O₁. Through point B₁, construct B₁ E perpendicular to the base ABCD at point E.

Question: Given the geometric solid shown in the diagram, the base ABC is an equilateral triangle with a side length of 4. The lateral face AA₁ C₁ C is a square, and the plane AA₁ C₁ C is perpendicular to the plane ABC. Point D lies on edge CC₁, with CD = (1/4) * CC₁, and BB₁ = 3CD. Determine the sine of the angle between line B₁D and plane AA₁ C₁ C.

Final Answer: $\sqrt{15}/5$



Original Diagram

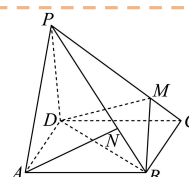


Auxiliary-line Diagram

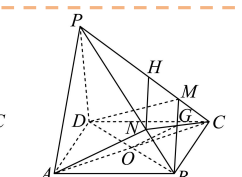
Auxiliary-line Description: Let M be the midpoint of AC and N be the midpoint of A₁ C₁. Then connect MN, BM, and NB₁. Through point B₁, construct B₁ H perpendicular to MN, intersecting MN at point H, then connect DH.

Question: As shown in the diagram, consider the quadrilateral pyramid P - ABCD, where the base ABCD is a parallelogram. Points M and N are located on segments PC and PB, respectively. Given that PM:MC = 3:1 and AN // plane BDM, determine the ratio PN:NB.

Final Answer: 2



Original Diagram

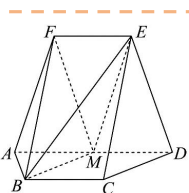


Auxiliary-line Diagram

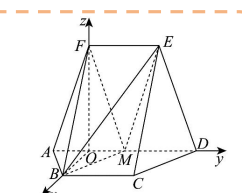
Auxiliary-line Description: Connect AC, which intersects BD at point O, connect CN, which intersects BM at point G, and then connect OG. Construct NH parallel to BM, intersecting PC at point H.

Question: As shown in the diagram, in a pentahedron with vertices A, B, C, D, E, quadrilaterals ABCD and ADEF are both isosceles trapezoids. It is given that EF is parallel to AD, BC is parallel to AD, AD = 4, AB = BC = EF = 2, ED = $\sqrt{10}$, FB = $2\sqrt{3}$, and M is the midpoint of AD. Find the sine of the dihedral angle F-BM-E.

Final Answer: $4\sqrt{3}/13$



Original Diagram

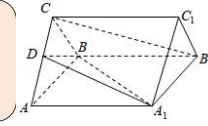


Auxiliary-line Diagram

Auxiliary-line Description: Draw BO perpendicular to AD intersecting AD at O, and connect OF. Take point O as the origin, and let the lines OB, OD, and OF be the x-axis, y-axis, and z-axis, respectively, to establish the three-dimensional Cartesian coordinate system O - xyz.

Figure 7: Representative examples from the AuxSolidMath dataset.

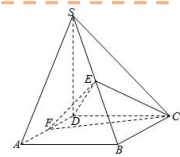
Question: As shown in the diagram, in the regular triangular prism $ABC - A_1 B_1 C_1$, the side length of the base is 2, and the lateral edge length is $\sqrt{3}$. D is the midpoint of AC. Find the volume of the triangular pyramid $D - A_1 C_1 B$.



Solution: [AUX]1. Construct auxiliary lines: Take the midpoint E of BC_1 , and connect $A_1 E$ and $D_1 E [AUX]$

Determine parallel lines: Since $ABC - A_1 B_1 C_1$ is a regular triangular prism, $AB \parallel C_1 D_1$ and $AB = C_1 D_1$. So quadrilateral $ABC_1 D_1$ is a parallelogram.
3. Identify equal lengths: Given the side length of the base is 2 and the lateral edge length is $\sqrt{3}$, triangle $C_1 DC$ is equilateral with side length 2.
4. Calculate the volume: Since $ABC - A_1 B_1 C_1$ is a regular triangular prism and triangle ABC is equilateral with side length 2, the height of the pyramid from D to the plane $A_1 C_1 B$ can be calculated as $\sqrt{3}$. The area of the triangular base $A_1 C_1 B$ is $(\sqrt{3})/4 * (2)^2 = \sqrt{3}$. Therefore, the volume of the pyramid is $(1/3) * \text{base area} * \text{height} = (1/3) * \sqrt{3} * \sqrt{3} = 1$.

Question: As shown in the diagram, in the quadrilateral pyramid $S - ABCD$, SD is perpendicular to the plane $ABCD$. The base $ABCD$ is a rhombus, with E and F being the midpoints of SB and AD , respectively. If $\angle BAD = 60^\circ$, $SD = 4$, and $AB = 2$, find the volume of the triangular pyramid $C - DEF$.



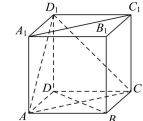
Solution: [AUX]1. Construct auxiliary lines: Take the midpoint H of AB , and connect DH . [AUX] 2. Since $\angle BAD = 60^\circ$ and $AB = AD = 2$, triangle ABD is equilateral.
3. Since H is the midpoint of AB, $AH = 1$. By Pythagoras theorem in right triangle ADH , $DH = \sqrt{(AD^2 - AH^2)} = \sqrt{(2^2 - 1^2)} = \sqrt{3}$.
4. Since $ABCD$ is a rhombus with $AB = BC = CD = DA = 2$ and $\angle ADC = 120^\circ$, we can calculate DC . Using cosine rule in triangle ADC , $DC^2 = AD^2 + AC^2 - 2*AD*AC*\cos(120^\circ) = 2^2 + (2^2) - 2*2*2*\cos(\pi/3) = 4 + 4 - 4 = 4$. So $DC = 2$.
5. Triangle CDE has vertices: C, D, E. E is the midpoint of SB. Since S is the apex and $SD \perp$ plane $ABCD$, plane $SAB \perp$ plane $ABCD$. Therefore, $DE \perp$ plane $ABCD$. Since CH lies in plane $ABCD$, we conclude $DE \perp CH$.
6. Since $AB = BC = CD = DA = 2$, and H is the midpoint of AB, $AC \perp BH$. Similarly, since $CD \perp DA$ (because $AD^2 + CD^2 = 2^2 + 1^2 = 5$, $AC^2 = 2^2 - 1^2 = 3$) and $DC = 2$, we can deduce $CH \perp CD$. Thus $CH \perp$ plane CDE .
7. The area of triangle CDE is:

$$\text{Area}(CDE) = (1/2) * DC * DE = (1/2) * 2 * 2 = 2$$
.
8. The height of the pyramid $C - DEF$ is CH . We need to find CH . In triangle CDB , $DB = 2\sqrt{2}$ (by Pythagoras theorem). So $CH = AC \sin(60^\circ) = 2 * (\sqrt{3}/2) = \sqrt{3}$.
9. The volume of pyramid $C - DEF$ is:

$$\text{Volume}(C-DEF) = (1/3) * \text{Area}(CDE) * CH = (1/3) * 2 * \sqrt{3} = \sqrt{3}/3$$
.

Final Answer: $\sqrt{3}/3$.

Question: As shown in the diagram, the edge length of the cube $ABCD - A_1 B_1 C_1 D_1$ is 2. Find the sine of the angle between line BD and plane ACD_1 .



Solution: [AUX]1. Establish coordinate system: Take point D as the origin, and let the lines DA , DC , and DD_1 be the x-axis, y-axis, and z-axis, respectively, to establish the three-dimensional Cartesian coordinate system $D-xyz$. [AUX]

Determine coordinates of points: Since the edge length of the cube $ABCD - A_1 B_1 C_1 D_1$ is 2, we have the coordinates of the vertices as follows:
1. $D = (0, 0, 0)$
2. $A = (2, 0, 0)$
3. $C = (0, 2, 0)$
4. $B = (2, 2, 0)$
5. $D_1 = (0, 0, 2)$
6. $A_1 = (2, 0, 2)$
7. $C_1 = (0, 2, 2)$
8. $B_1 = (2, 2, 2)$.
Find the coordinates of point E: E is the midpoint of BD. The coordinates of B are $(2, 2, 0)$ and D are $(0, 0, 0)$. The midpoint E is the average of the coordinates of B and D:

$$E = ((2+0)/2, (2+0)/2, (0+0)/2) = (1, 1, 0)$$
.
Find the vector BD : We have point B = $(2, 2, 0)$ and point D = $(0, 0, 0)$.

$$\text{Vector } BD = D - B = (0 - 2, 0 - 2, 0 - 0) = (-2, -2, 0)$$
.
Find a normal vector to the plane ACD_1 : To find the normal vector, we need two vectors in the plane ACD_1 .

$$\text{Vector } AC = C - A = (0 - 2, 2 - 0, 0 - 0) = (-2, 2, 0)$$
.

$$\text{Vector } AD_1 = D_1 - A = (0 - 2, 0 - 0, 2 - 0) = (-2, 0, 2)$$
.
Normal vector n to the plane ACD_1 is the cross product of AC and AD_1 :

$$n = AC \times AD_1 = (-2, 2, 0) \times (-2, 0, 2) = (2*2 - 0*0, 0*(-2) - (-2)*2, (-2)*0 - 2*(-2)) = (4, 4, 4)$$
.
We can take a simpler normal vector by dividing by 4, so we can take $n = (1, 1, 1)$.
Calculate the sine of the angle between line BD and plane ACD_1 : The sine of the angle θ between line BD and plane ACD_1 is given by the absolute value of the cosine of the angle between vector BD and normal vector n .

$$\sin(\theta) = |\cos(\text{angle between } BD \text{ and } n)| = |(BD \cdot n) / (|BD| * |n|)|$$
.

$$BD \cdot n = (-2, -2, 0) \cdot (1, 1, 1) = (-2)(1) + (-2)(1) + (0)(1) = -2 - 2 + 0 = -4$$
.

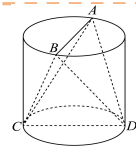
$$|BD| = \sqrt{((-2)^2 + (-2)^2 + 0^2)} = \sqrt{8} = 2\sqrt{2}$$
.

$$|n| = \sqrt{(1^2 + 1^2 + 1^2)} = \sqrt{3}$$
.

$$\sin(\theta) = |-4 / (2\sqrt{2} * \sqrt{3})| = |-4 / (2\sqrt{6})| = |-2/\sqrt{6}| = 2/\sqrt{6} = 2\sqrt{6}/6 = \sqrt{6}/3$$
.

Final Answer: $\sqrt{6}/3$.

Question: As shown in the diagram, the diameter of the base of the cylinder is 3, and the slant height is 4. AB and CD are the diameters of the upper and lower bases of the cylinder, respectively, and $AB \perp CD$. Find the volume of the triangular pyramid A-BCD.



Solution: [AUX]1. Construct auxiliary lines: Take the midpoint M of AB, and connect MD and MC. [/AUX]

Determine the base area of the triangular pyramid: Since $AB \perp CD$ and $AB = CD = 3$ (diameter), the area of the triangular base ABCD is given by:

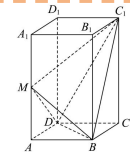
$$\text{Area} = (1/2) * AB * CD = (1/2) * 3 * 3 = 4.5$$

Determine the height of the pyramid: The height of the triangular pyramid A-BCD is the perpendicular distance from A to the plane BDC. Given that $AB \perp$ plane BDC, the height is AB itself, which is given as 4 (slant height).

$$\text{Volume} = (1/3) * \text{Area of base} * \text{Height} = (1/3) * 4.5 * 4 = 6$$

Final Answer: 6.

Question: As shown in the diagram, in the regular quadrilateral prism ABCD-A₁B₁C₁D₁, M is the midpoint of AA₁, AB = 2, AA₁ = 4. Find the cosine value of the dihedral angle C₁-BD-M.

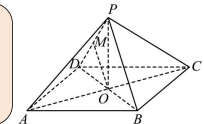


Solution: [AUX]1. Establish coordinate system: Take point D as the origin, and let the lines DA, DC, and DD₁ be the x-axis, y-axis, and z-axis, respectively, to establish the three-dimensional Cartesian coordinate system D-xyz. [/AUX]

Determine coordinates of points: Since ABCD-A₁B₁C₁D₁ is a regular quadrilateral prism with base side length AB = 2 and height AA₁ = 4, we have the coordinates of the vertices as follows:
 $D = (0, 0, 0)$ $A = (2, 0, 0)$ $C = (0, 2, 0)$ $B = (2, 2, 0)$
 $D_1 = (0, 0, 4)$ $C_1 = (0, 2, 4)$ $A_1 = (2, 0, 4)$
M is the midpoint of AA₁, so $M = ((2+0)/2, (0+0)/2, (0+4)/2) = (2, 0, 2)$.
Find normal vectors of planes C₁BD and MBD:
For plane C₁BD, we need two vectors in the plane: C₁D and C₁B.
Vector C₁D = D - C₁ = (0, 0, 0) - (0, 2, 4) = (0, -2, -4).
Vector C₁B = B - C₁ = (2, 2, 0) - (0, 2, 4) = (2, 0, -4).
The normal vector n₁ of plane C₁BD is the cross product of C₁D and C₁B:
 $n_1 = C_1 D \times C_1 B = (0, -2, -4) \times (2, 0, -4) = ((-2)(-4) - (-4)(0), (-4)(2) - 0 * (-4), 0(0) - (-2)(2)) = (8, -8, 4)$.
We can take a simpler normal vector by dividing by 4, so n₁' = (2, -2, 1).
For plane MBD, we need two vectors in the plane: MB and MD.
Vector MB = B - M = (2, 2, 0) - (2, 0, 2) = (0, 2, -2).
Vector MD = D - M = (0, 0, 0) - (2, 0, 2) = (-2, 0, -2).
The normal vector n₂ of plane MBD is the cross product of MB and MD:
 $n_2 = MB \times MD = (0, 2, -2) \times (-2, 0, -2) = (2(-2) - (-2)(0), (-2)(-2) - 0(-2), 0(0) - 2(-2)) = (-4, 4, 4)$.
We can take a simpler normal vector by dividing by 4, so n₂' = (-1, 1, 1).
Calculate the cosine of the dihedral angle:
The cosine of the dihedral angle θ is the cosine of the angle between the normal vectors n₁' and n₂'.
 $\cos(\theta) = |(n_1' \cdot n_2') / (|n_1'| * |n_2'|)|$.
 $|n_1'| = \sqrt{(2^2 + (-2)^2 + 1^2)} = \sqrt{4 + 4 + 1} = \sqrt{9} = 3$.
 $|n_2'| = \sqrt{(-1)^2 + 1^2 + 1^2} = \sqrt{1 + 1 + 1} = \sqrt{3}$.
 $\cos(\theta) = |-3 / (3 * \sqrt{3})| = |-3 / (3\sqrt{3})| = |-1/\sqrt{3}| = 1/\sqrt{3} = \sqrt{3}/3$.

Final Answer: $\sqrt{3}/3$.

Question: In the quadrilateral pyramid P-ABCD, the quadrilateral ABCD is a rhombus, with AC and BD intersecting at point O. PA = PC, PB = PD, $\angle BAD = 60^\circ$, AB = 2, and M is the midpoint of segment PD. If the angle between line OM and plane ABCD is 60° , find the sine of the dihedral angle between plane PAD and plane PBC.



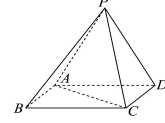
Solution: [AUX]1. Establish coordinate system: Take point O as the origin, and let the lines OA, OB, and OP be the x-axis, y-axis, and z-axis, respectively, to establish the three-dimensional Cartesian coordinate system O-xyz. [/AUX]

Determine coordinates of points: Since the rhombus ABCD has side length 2 and $\angle BAD = 60^\circ$, triangle ABD is equilateral, and triangle BCD is also equilateral. The diagonals AC and BD are perpendicular bisectors of each other. Given AB = 2, we have AO = OC = 1 and BO = OD = $\sqrt{(2^2 - 1^2)} = \sqrt{3}$. Thus, the coordinates are:
 $O = (0, 0, 0)$ $A = (1, 0, 0)$ $C = (-1, 0, 0)$ $B = (0, \sqrt{3}, 0)$
Since PA = PC and PA = $\sqrt{(1-0)^2 + (0-\sqrt{3})^2 + k^2}$, PC = $\sqrt{(-1-0)^2 + (0-\sqrt{3})^2 + k^2}$. Squaring both PA and PC and equating them:
 $(1-h)^2 + k^2 = (-1-h)^2 + k^2$ $h = 0$
Substituting h = 0 into PA² = (1-0)² + (0-0)² + k² = 1 + k² = 1 + (h²) = PB². So z coordinate of P = OM = $\sin(60^\circ) = \sqrt{3}/2$. M is the midpoint of PD, M = ((0+0)/2, (0+0)/2, $\sqrt{3}/2$) = (0, 0, $\sqrt{3}/2$).
Find normal vectors of plane PAD and plane PBC:
For plane PAD, we need vectors PA and PD.
Vector PA = A - P = (1, 0, - $\sqrt{3}$).
Vector PD = D - P = (0, - $\sqrt{3}$, - $\sqrt{3}$).
Normal vector n₁ of plane PAD is the cross product of PA and PD:
 $n_1 = PA \times PD = (1, 0, -\sqrt{3}) \times (0, -\sqrt{3}, -\sqrt{3}) = (-3, \sqrt{3}, -\sqrt{3})$.
For plane PBC, we need vectors PB and PC.
Vector PB = B - P = (0, $\sqrt{3}$, - $\sqrt{3}$).
Vector PC = C - P = (-1, 0, - $\sqrt{3}$).
Normal vector n₂ of plane PBC is the cross product of PB and PC:
 $n_2 = PB \times PC = (0, \sqrt{3}, -\sqrt{3}) \times (-1, 0, -\sqrt{3}) = (-3, \sqrt{3}, \sqrt{3})$.
Calculate the cosine of the dihedral angle:
 $\cos(\theta) = |(n_1 \cdot n_2) / (|n_1| * |n_2|)|$.
 $|n_1| = \sqrt{(-3)^2 + (\sqrt{3})^2 + (-\sqrt{3})^2} = \sqrt{15}$.
 $|n_2| = \sqrt{(-3)^2 + (\sqrt{3})^2 + (\sqrt{3})^2} = \sqrt{15}$.
 $\cos(\theta) = |-3 / (\sqrt{15} * \sqrt{15})| = |-3 / 15| = 3 / 15 = 1 / 5$.
Calculate the sine of the dihedral angle:
 $\sin^2(\theta) = 1 - \cos^2(\theta) = 16 / 25$.
 $\sin(\theta) = \sqrt{16 / 25} = 4 / 5$.

Final Answer: $4/5$.

Figure 8: Successful cases generated by GeoVLMath-7B.

Question: As shown in the diagram, in the quadrilateral pyramid P-ABCD, the base ABCD is a square, PAD is an equilateral triangle, and $PC = AC$. Find the sine of the angle between line PB and plane PCD.

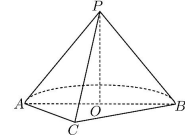


Ground Truth: $\sqrt{6}/4$

Analysis: The A-xyz coordinate system is incorrectly established—**AP is not orthogonal to AB or AD**, violating the pairwise orthogonality required for a three-dimensional Cartesian system. Consequently, the coordinates assigned to points and lines are invalid, leading to an incorrect final answer.

Solution: **[AUX1. Establish coordinate system: Take point A as the origin, and let the lines AB, AD, and AP be the x-axis, y-axis, and z-axis, respectively, to establish the three-dimensional Cartesian coordinate system A-xyz. [/AUX]** **n2.** Determine the coordinates of the vertices: Let the side length of the square ABCD be 2. Since A is the origin, $A = (0, 0, 0)$. As AB is along the x-axis and B is to the right of A with length 2, $B = (2, 0, 0)$. As AD is along the y-axis and D is above A with length 2, $D = (0, 2, 0)$. Since ABCD is a square, $C = (2, 2, 0)$. As PA is a line from A in the z-direction upwards and triangle PAD is an equilateral triangle with side length 2, the height from P to the base ABCD must be $\sqrt{(2^2 - 1^2)} = \sqrt{3}$. So, $P = (0, 0, \sqrt{3})$. **n3.** Find the vector PB: We have $P = (0, 0, \sqrt{3})$ and $B = (2, 0, 0)$. The vector $PB = B - P = (2, 0, 0) - (0, 0, \sqrt{3}) = (2, 0, -\sqrt{3})$. **n4.** Find the normal vector of the plane PCD: We need two vectors in the plane PCD, for example, vector PC and vector PD. **n** Vector $PC = C - P = (2, 2, 0) - (0, 0, \sqrt{3}) = (2, 2, -\sqrt{3})$. **n** Vector $PD = D - P = (0, 2, 0) - (0, 0, \sqrt{3}) = (0, 2, -\sqrt{3})$. **n** The normal vector n of the plane PCD is the cross product of PC and PD: **n** $PC \times PD = (2, 2, -\sqrt{3}) \times (0, 2, -\sqrt{3}) = (2 * (-\sqrt{3}) - (-\sqrt{3}) * 2, (-\sqrt{3}) * 0 - 2 * (-\sqrt{3}), 2 * 2 - 2 * 0) = (-2\sqrt{3} + 2\sqrt{3}, 0 + 2\sqrt{3}, 4 - 0) = (0, 2\sqrt{3}, 4)$. **n** To take a simpler normal vector, we can use $n' = (0, \sqrt{3}, 2)$. **n5.** Calculate the sine of the angle between line PB and plane PCD: The sine of the angle θ between line PB and plane PCD is given by the absolute value of the cosine of the angle between vector PB and normal vector n' : **n** $\sin(\theta) = |\cos(\text{angle between } PB \text{ and } n')| = |(PB \cdot n') / (|PB| * |n'|)|$. **n** $PB \cdot n' = (2, 0, -\sqrt{3}) \cdot (0, \sqrt{3}, 2) = 2 * 0 + 0 * \sqrt{3} + (-\sqrt{3}) * 2 = -2\sqrt{3}$. **n** $|PB| = \sqrt{(2^2 + 0^2 + (-\sqrt{3})^2)} = \sqrt{4 + 0 + 3} = \sqrt{7}$. **n** $|n'| = \sqrt{(0^2 + (\sqrt{3})^2 + 2^2)} = \sqrt{0 + 3 + 4} = \sqrt{7}$. **n** $\sin(\theta) = |-2\sqrt{3} / (\sqrt{7} * \sqrt{7})| = |-2\sqrt{3} / 7| = 2\sqrt{3} / 7$. **n** **Final Answer: $2\sqrt{3}/7$** .

Question: As shown in the diagram, the given solid consists of half of a cone and a triangular pyramid. The base of the cone is a circle with center O and radius 1, and the height of the cone satisfies $PO = 2$. The triangular pyramid P-ABC has its base ABC as an isosceles right triangle, where AB is the hypotenuse and coincides with the diameter of the cone's base circle. The base ABC lies on the same plane as the cone's base. Determine the angle between line PC and plane ABC.



Ground Truth: $\arctan 2$

Analysis: The generated auxiliary-line description **leaves the geometric configuration unchanged**. Consequently, the subsequent reasoning proceeds from a spurious auxiliary premise rather than from added geometric constraints, leading to an incorrect final answer.

Solution: **[AUX1. Construct auxiliary lines: Take the midpoint M of AB, and connect OM. [/AUX]** **n2.** Identify perpendicularity: Since O is the center of the circle, $OM \perp AB$. Also, $PO \perp OM$ because PO is the height of the cone and O is on the base circle. Since $AB \cap PO = O$, and AB and PO are in plane PAB, we conclude $OM \perp$ plane PAB. **n3.** Determine angle: The angle between line PC and plane ABC is the angle between line PC and its projection onto plane ABC. Since $OM \perp$ plane PAB, the projection of point P onto plane ABC lies on line OM. The projection of line PC onto plane ABC is segment AC. **n4.** Calculate angle: To find the angle between line PC and plane ABC, we need to find the sine of the angle. Given $PO = 2$ and $OA = 1$, we have $AC = \sqrt{(PA^2 - AO^2)} = \sqrt{(2^2 - 1^2)} = \sqrt{3}$. **n** **Final Answer: $\arcsin(\sqrt{3}/3)$**

Figure 9: Failure cases generated by GeoVLMath-7B.